

Short communication

Invariant in variants

Cong Liu^{a,b}, Chen-Wu Wu^{a,*}^a Institute of Mechanics, Chinese Academy of Sciences, Beijing 100190, China^b School of Engineering Science, University of Chinese Academy of Sciences, Beijing 100049, China

A B S T R A C T

The coronavirus Covid-19 mutates quickly in the pandemic, leaves people struggling to verify and improve the effectiveness of the vaccine based on biochemistry. Is there any physical invariant in the variants of such kind of pathogen that could be taken advantage to ease the tensions? To this point, extensive numerical experiments based on continuity mechanics have been accomplished to discover the consistent vibration modes and the range of natural frequency of coronavirus Covid-19. Such invariant could help us in developing some flexible technique to deactivate the coronavirus, like as resonantly breaking the viral spike by ultrasound wave. The fundamental mechanisms governing such process are demonstrated via solving the coupled acoustic wave and elastic dynamic equations, after which the practical strategies are proposed to efficiently realize the technique concept.

1. Introduction

The war has been going on, between human and virus, focusing on the coronavirus Covid-19 since early 2020 [1–3]. The tiny virus has been causing big trouble and keeps changing into various mutants, of which at least ten variants (α , β , γ , δ , η , ι , κ , λ , μ , ν) have been designated by WHO up to Nov 26, 2021, all of which have been bringing so much sickness, injury and death to mankind [4,5]. The human immune system could mostly conquer the invasive coronavirus autonomously with the aid of effective vaccine, although which require continuing update of the vaccines to produce enough antibody [6–8]. Or else, we could actively deactivate the coronavirus in the ambient air [9] surrounding animals and human beings to largely suppress the infection probability. This could be realized by chemical way, like spraying strong acid/alkali disinfectant or physical approaches, such as electromagnetic wave/ultrasonic wave irradiation [10–13]. Although, the overuse of chemical disinfectant is regarded to be partially responsible for accelerating the mutation of a large group of pathogens and increasing their antibiotic-resistances [14]. In contrast, it is almost impossible for a virus to mutate to escape from the attack by physical means, no matter through thermal or mechanical effects [10,11] that could permanently devitalize the coronavirus via breaking its spike, membrane or even nucleic acid core that exists in the various form of mechanical structures [10,15]. Among the potential mechanical methods, the ultrasonic inactivation is generally regarded as one of the mostly promising options because of its peculiar advantages [12,16–18].

Despite the facts that the ultrasound wave could also be utilized to heat an object with thermally dissipating the mechanical energy

transported in wave form [15], ultrasound wave directly exciting the mechanical resonance of the virion would extremely deform and rupture its spike or envelope to quickly deactivate the virus [16–18]. Of course, such mechanical resonance of the viral structure with the stimulating ultrasound wave source relies fundamentally on the prerequisite that the frequency of the ultrasound wave is close enough to one of the natural frequencies of the viral structure [17,18], which is critical to avoid excessive energy loss due to the phase discrepancy [19]. Therefore, accurate predictability of the natural frequency of the virion is figured on to develop any practical appliance that always operates in certain range of physical parameters such as frequency and power. This implies that the possible diversification in natural frequency of the virions would be a potential obstacle blocking the way of ultrasonic disinfection of coronavirus Covid-19. However, the effects of the geometry deviation and environment change on the natural vibration modes have not been included in the previous investigations [17,18], almost all of which only provides certain natural frequencies. In fact, the aforementioned uncertainty would inevitably lead to some range in natural frequency of such kind of microbiology. Therefore, the corresponding practical operation tactics should be developed to optimize the dynamic responses of the virions with natural frequency within some predicted range. We firstly study the vibration modes of the viral structure with massive computations to involve the variations in both geometry patterns [20,24,25] and mechanical properties [13,21,23] of the viral mutants. Then, we calculate the stimulated stress field in the virion excited by the ultrasound waves of specific frequency as well as of varied frequency based on direct solution of the coupled equations governing acoustic and elastic fields. The present study involves the actual

* Corresponding author.

E-mail address: chenwuwu@imech.ac.cn (C.-W. Wu).<https://doi.org/10.1016/j.ultras.2022.106749>

Received 9 January 2022; Received in revised form 25 March 2022; Accepted 4 April 2022

Available online 8 April 2022

0041-624X/© 2022 Elsevier B.V. All rights reserved.

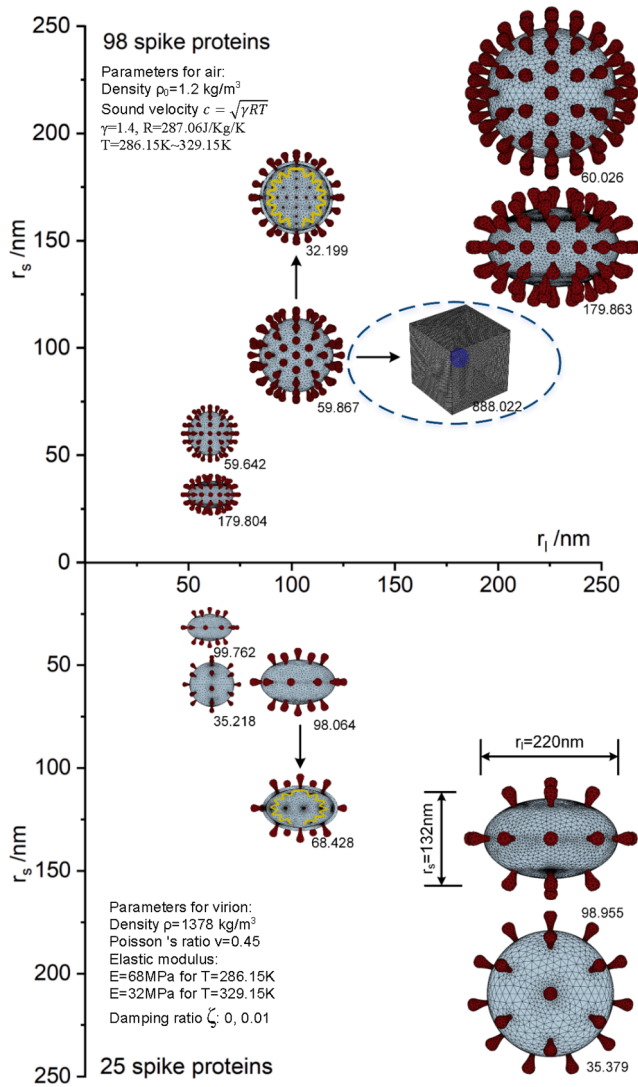


Fig. 1. Sketch of the model on coronavirus Covid-19 with the lower part representing the virus with 25 spike proteins and upper part with 98 spike proteins, along with the parameters of the air and viral material used in computation [11,12,17,18,27].

interactions between the ultrasonic wave and viral structure and are superior in methodology to reveal physical reality over previous work [17,18]. Finally, we propose and verify the strategies of frequency scanning to efficiently realize the technologic concept.

2. Model description

The main mechanical body of the coronavirus Covid-19 in geometry commonly consists of an ellipsoidal/spherical envelope shell and most probably 25–98 solid spikes nearly symmetrically distributed on the viral envelope [18,20,23–25] as shown in Fig. 1, wherein the spherical envelope could also be approximated by a regular icosahedron [24]. Moreover, the axis length of the viral envelope is statistically revealed to be in the range of (60 nm, 220 nm), attached to which both the envelope thickness and the spike height are commonly in stable ratios to the average axis length [24–26]. Such geometrical consistency of the virions truly demonstrates kind of mathematical similarity in the various mutants of the virus. Being mechanically made up of strong and tough protein, the viral envelope encloses and protects the carriers of genetic information, DNA/RNA while the spikes work as intruder and deliverer of the DNA/RNA into the target animal cells [8,20,27–29].

Table 1

Physical parameters of the coronavirus and air [18,20–23].

Virus	Density [ρ]	Poisson's ratio [ν]	Elastic modulus [E]	Damping ratio [ζ]
	1378 kg/m ³	0.45	68 MPa for temperature $T = 286.15 \text{ K}$ 32 MPa for temperature $T = 329.15 \text{ K}$	0–0.01
Air	Density [ρ]	Speed of sound [c]		Temperature [T]
	1.2 kg/m ³ (293.15 K, 1 atm)	$\sqrt{\gamma RT}$, $\gamma = 1.4$, $R = 287.06 \text{ J Kg}^{-1} \text{ K}^{-1}$		286.15–329.15 K

Therefore, breaking the viral spike would prohibit the invasion into animal cell and hence the injection of the genetic information, which could be realized rapidly via imposing the ultrasound wave [18] on the virions if only the excitation frequency match well the natural frequency of the viral structure [11,18]. From the point of view of physics, the deformation as well as stress would accumulate due to resonant excitation appears in a synchronized status and fractures arise once the stress approaches to the ultimate strength of the solid material [30,31]. Accordingly, the key determinant is whether the natural frequency ω can be accurately evaluated, which could be completed by solving the characteristic equations governing the dynamic behaviors of the virions.

The present study mainly involves the materials of air and the virions, of which the physical parameters, such as density ρ , ratio of specific heat capacity γ , gas constant R , damping ratio ζ , Poisson's ratio ν and elastic modulus E for typical temperature levels if necessary have been cited from literature [18,20–23] and listed in Table 1.

Note that the damping ratio in Table 1 is assumed to be in the range of (0, 0.01) to investigate the kinetic energy dissipation due to damping quantitatively, which in magnitude has covered more than enough the value interval of damping ratio adopted in previous work [23].

The three-dimensional geometric models of the virions have been completed in CAD software through the three key procedures of shell feature generation, spike feature generation, and distributed assembly based on the statistically averaged geometrical dimensions referred to the reported data [24–29].

All of the coupled differential equations have been directly solved by Finite Element Method [32] to reveal the real-time energy transfer and conversion, accompanied with the reflection and absorption of the incident acoustic waves upon the virion surfaces. In comparison, the previous work [17,18] applied simplified pressure or force to the viral structure without including the interaction between the ultrasonic wave and the viral structure. The cubic computation domain of size $1 \mu\text{m} \times 1 \mu\text{m} \times 1 \mu\text{m}$ is accordingly discretized into nearly 1 million subdomains formed by the mesh grids as sketched in Fig. 1 (partitioned symmetrically), which also includes the sketches of typical mesh grids of the virions.

Natural frequencies and vibration modes are determined by the characteristic equations in structural dynamics (Eq. (1)).

$$-\rho\omega^2\mathbf{u} = \nabla \cdot \boldsymbol{\sigma} \quad (1)$$

Wherein, ρ is the viral material, the operator $\nabla = [\frac{\partial}{\partial x}, \frac{\partial}{\partial y}, \frac{\partial}{\partial z}]^T$ with the superscript T representing the transpose form of a vector, ω is the angular frequency, the eigenvectors $\mathbf{u}(x,y,z,t) = \mathbf{u}(x,y,z)e^{i\omega t}$ represents the displacement field for the case of time-harmonic response and (x, y, z) are the Cartesian coordinates.

The displacement field \mathbf{u} determines the stress field $\boldsymbol{\sigma}$ through the geometrical equations (Eq. (2)) governing strain-displacement relationship and constitutive equations (Eq. (3)) governing stress-strain relationship [30].

$$\varepsilon_{ij} = \frac{1}{2} \left(\frac{\partial u_i}{\partial x_j} + \frac{\partial u_j}{\partial x_i} \right); i, j = x, y, z \quad (2)$$

Wherein, ε_{ij} are the components of strain tensor, u_i are the displacement components.

$$\sigma_{ii} = \frac{E}{(1+\nu)(1-2\nu)} [(1-\nu)\varepsilon_{ii} + \nu(\varepsilon_{jj} + \varepsilon_{kk})]; \sigma_{ij} = \frac{E}{1+\nu} \varepsilon_{ij}; i, j, k = x, y, z \quad (3)$$

With E being the elastic modulus of materials, ν the Poisson's ratio and (x, y, z) are the Cartesian coordinates.

The elastic dynamic equations (Eq. (4)) govern the movement, deformation and hence stress distribution of the virus particle, while the acoustic wave equation (Eq. (5)) describes the propagation of the ultrasound wave in the media.

The boundary conditions (Eq. (6)) are applied to the interface between the virion and the air to follow the law of conservation. The boundary condition (Eq. (7)) is acted upon the side $x = 0$ of the cubic volume of air with side length of $1 \mu\text{m}$, at the center of which located the virus particle and the other sides of which is assumed as nonreflecting boundaries. The law of conservation and rule of continuity in energy and momentum are applied to the virus surface that acts as the interface between the virus particle and surrounding air environment.

$$\rho \frac{\partial^2 \mathbf{u}}{\partial t^2} = \nabla \cdot \boldsymbol{\sigma} \quad (4)$$

$$\frac{1}{\rho c^2} \left(\frac{\partial^2 p}{\partial t^2} \right) + \nabla \cdot \left(-\frac{1}{\rho} \nabla p \right) = 0 \quad (5)$$

$$-\mathbf{n} \cdot \left(-\frac{1}{\rho c} (\nabla p) \right) = -\mathbf{n} \cdot \mathbf{u}_t \quad (6)$$

$$p|_{x=0} = p_0 \sin(\omega_e t) \quad (7)$$

Wherein, ρ is the mass density of virion or air, t is the time, c is the wave velocity in the air enclosing the virion, \mathbf{u} is the displacement field and its' second partial derivative to time \mathbf{u}_t means acceleration; \mathbf{n} is the unit normal vectors, p is the acoustic pressure developed by the ultrasound wave, the acoustic pressure exerted on the domain boundary $x = 0$ is assumed as $p(t) = p_0 \sin(\omega_e t)$ and ω_e is the angular frequency of the ultrasonic wave.

The amplitude p_0 of the acoustic pressure induced by the ultrasonic wave was set as unit magnitude "1" to normalize the numerical results considering the intrinsic linearity of the problem described by the elastic and acoustic equations, which would be retained even the complex interaction between the incident ultrasound and the virus particle is involved herein. The propagation of the ultrasound, including reflection and refraction upon the surface of virus particle, could be accurately enough approximated with the above linear equations for the cases of specified temperature as the pressure is as moderate as discussed in the present study. This would lead to a constant sound wave velocity for any specified temperature, c independent of the pressure in the air [30,31].

The alteration ways of the frequency $\omega_e/\omega_0^{(1)}$ with time utilized in exciting the swing vibration of the viral spike could be expressed by a function of time, t as (Eq. (8)) and (Eq. (9)).

$$\omega_e/\omega_0^{(1)} = (0.5 + 1.5t/180) \quad (8)$$

for the case of continuously change and.

$$\begin{aligned} \omega_e/\omega_0^{(1)} &= 2.0 \text{ for } 135 < t/\text{ns} \leq 180; \\ \omega_e/\omega_0^{(1)} &= 1.5 \text{ for } 90 < t/\text{ns} \leq 135; \\ \omega_e/\omega_0^{(1)} &= 1.0 \text{ for } 45 < t/\text{ns} \leq 90; \end{aligned}$$

$$\omega_e/\omega_0^{(1)} = 0.5 \text{ for } 0 < t/\text{ns} \leq 45 \quad (9)$$

for the case of stepwisely change.

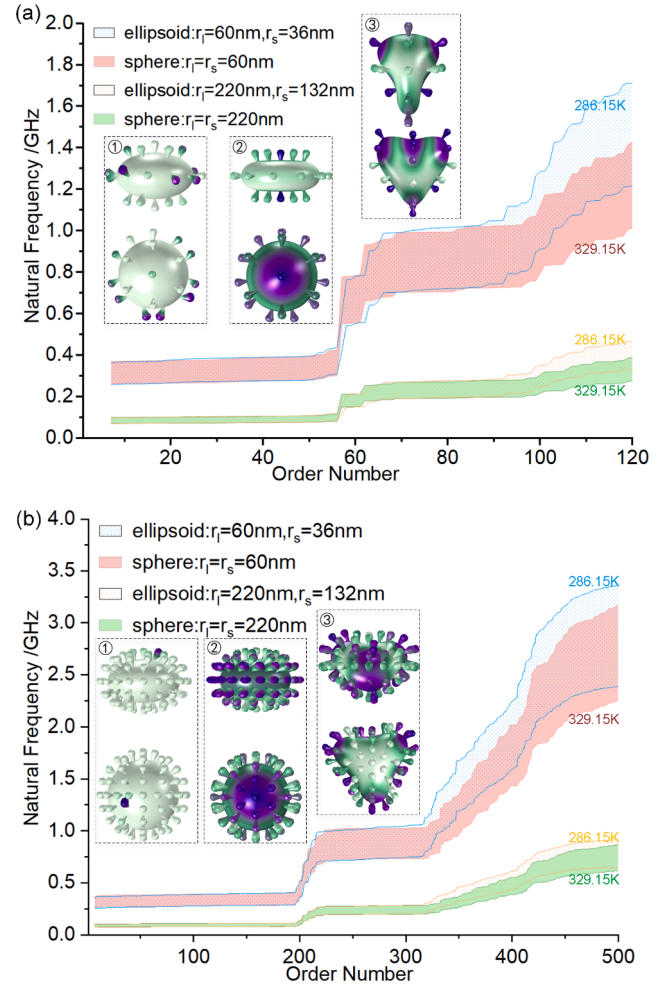


Fig. 2. Natural frequencies of the virions of temperature in the range of (286.15 K, 329.15 K) with (a) the upper representing the virus with 25 spike proteins (up to 120th order) and (b) the lower with 98 spike proteins (up to 500th order), along with the first three distinctive vibration modes.

3. Modal responses

The typical vibration shapes along with natural frequency of the virus Covid-19, as shown in Fig. 2 have been calculated up to 120 and 500 orders for the viral configurations with 25 spikes and 98 spikes, respectively. Considering the fact that temperature fluctuation would change stiffness of the viral structure and therefore change the Eigen solutions to characteristic equation, the results on natural frequency have been maintained through the temperature range from 286.15 K to 329.15 K and form the continuous strips of data.

It is revealed that the vibration modes of spike swing occupy up to about 50 orders of the vibration shapes of the virus with 25 spikes and up to about 196 orders of the virus with 98 spikes, respectively. The envelope vibration is negligible before the critical orders, which is the case regardless of the viral geometry or temperature level. It is indicated that the natural frequencies, $\omega_0^{(1)}/2\pi$ that associated with spike swing, basically fall into the ranges of (0.07 GHz, 0.12 GHz) or (0.26 GHz, 0.44 GHz), in which both ratios of upper bound to lower bound are less than 2. Such an invariant in the natural frequency of the virions Covid-19 would provide a great maneuverability in choosing ultrasonic wave frequency to stimulate spike swing.

It is also revealed in Fig. 2 that the viral envelop size determines the natural frequency of the virions and divides the frequency data into two separated regions, while as the effect of the envelop shape is relatively ignorable especially for the modes of spike swing.

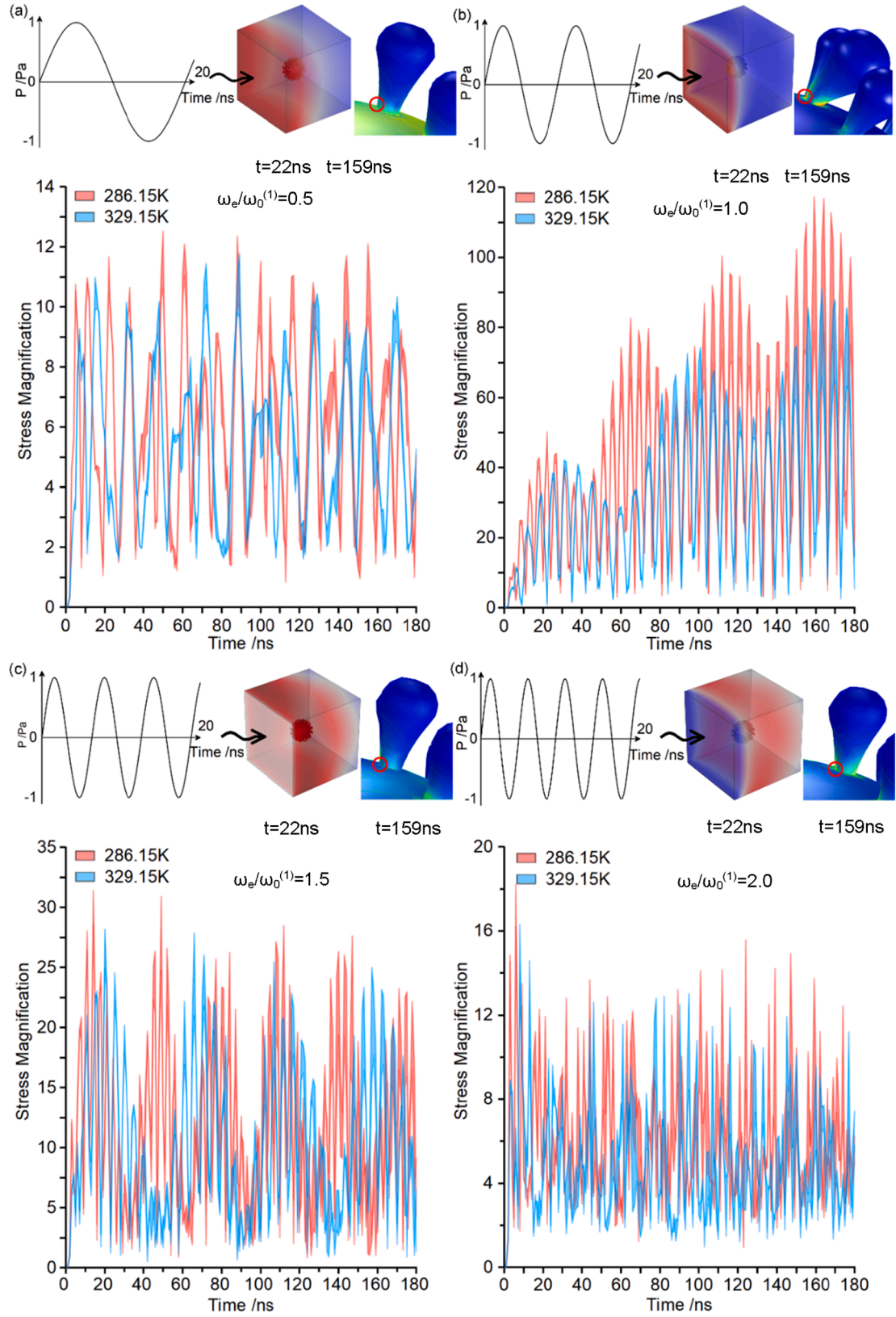


Fig. 3. Stress magnification around the root of the swung spike excited by ultrasound wave of single frequency ω_e that (a) 0.5, (b) 1.0, (c) 1.5 and (d) 2.0 times the first natural frequency of the virus $\omega_0^{(1)}$, along with acoustic pressure, stress field and the wave profiles of the ultrasonic waves for the cases of temperature $T = 286.15$ K.

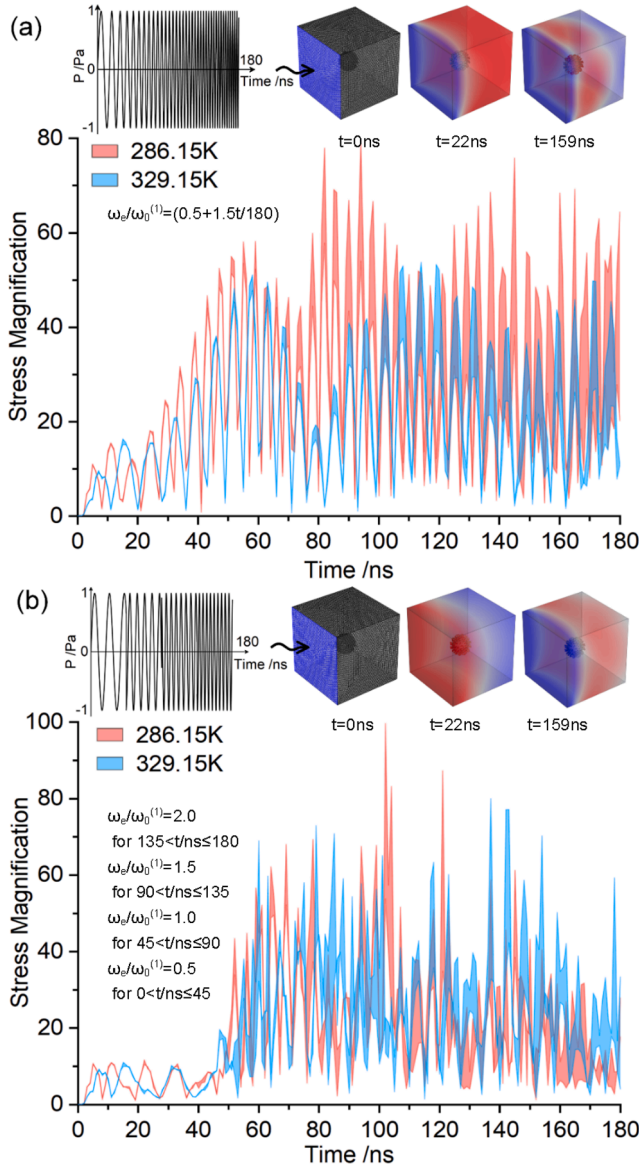


Fig. 4. Stress magnification around the root of swung spike excited by ultrasound wave of frequency ω_e that change (a) continuously and (b) step-wisely with time, along with acoustic pressure, stress field and the initial wave profiles of the ultrasonic waves for the cases of temperature $T = 286.15$ K.

4. Dynamic responses

Without loss of generality, the dynamic responses of the spherical Covid-19 virions of diameter 220 nm and 98 spikes to the action of planar ultrasound wave $P = P_0 \sin(t\omega_e)$ have been obtained via solving simultaneously the coupled elastic dynamic and acoustic wave equations.

The strategies to excite the spike swing in the virions are demonstrated to apply ultrasound wave with ω_e being fixed, continuously-increased or stepwisely-increased, for which the wave profiles along with acoustic pressure and stress fields are plotted in the top of **Figs. 3 and 4**. **Figs. 3 and 4** mainly present the stress magnifications σ_m/P_0 versus time with σ_m being the maximum von-Mises equivalent stress around the spike root, which would break once σ_m equals to its' ultimate strength according to fracture theory [30].

Results on each case in **Figs. 3 and 4** have been separately plotted for the two temperature levels, 286.15 K (in bright color) and 329.15 K (in dark color) in different data strip whose thickness, the height difference

in the values of upper bound and lower bound reflects thermal dissipation of mechanical energy due to damping. Of course, the damping would suppress the stress magnification in a whole while lead to temperature elevation in virions. It is found that the peak value of stress magnification is inversely related to temperature as temperature elevation always result in softening the material, namely reduce elastic modulus of the material.

The four groups of curves in **Fig. 3(a)**, **(b)**, **(c)** and **(d)** depict $\sigma_m/P_0 \sim t$ for the cases that the ratio of excitation frequency ω_e of ultrasonic waves to the first natural frequency of the virion, $\omega_e/\omega_0^{(1)}$ is 0.5, 1.0, 1.5 and 2.0 in sequence. It is obviously shown in **Fig. 3(b)** that the stress magnifications would be accumulated cyclically when ω_e equals to $\omega_0^{(1)}$, which indicates an apparent resonance stimulation. In this case, the peak stress magnification is over 100 before $t = 120$ ns if damping ratio is 0 and still over 70 at the instant $t = 100$ ns even if damping ratio is 0.01. That means, the maximum equivalent stress, $70 \times P_0$ around the spike root would approach to its' ultimate strength, about 0.141 MPa [13,18] within 100 Nano seconds even if the pressure altitude P_0 of the ultrasound wave is only 2 kPa, which is truly very low [31]. Meanwhile, the stress magnification would not be accumulated if the frequency ratio $\omega_e/\omega_0^{(1)}$ deviate from 1.0 as shown in **Fig. 3(a)**, **(c)** and **(d)** as the input mechanical energy would be largely lost.

Encouragingly, we found that a large magnitude of stress magnification always arises within 180 ns if change the frequency ratio $\omega_e/\omega_0^{(1)}$ from 0.5 to 2.0 during excitation, no matter continuously as in **Fig. 4(a)** or stepwisely as in **Fig. 4(b)**. Moreover, the excitation via continuously changing frequency leads to a relatively smooth change in the peak values of stress magnification, while step-wisely changing results in relatively higher peak values with more rapid fluctuations. The peak stress magnifications within 180 ns are over 70 by both strategies for the cases of temperature 286.15 K, in comparison the peak stress magnifications are over 50 for temperature 329.15 K. The complete statistics show that the peak stress magnifications around the roots of all of the 98 spikes under any condition exceed 10 within 180 ns, which still only request an ultrasonic wave of intensity lower than 15 kPa to break the viral spike.

5. Conclusions

The spike swing is found to be constantly the lowest order vibration mode of the variants of the coronavirus Covid-19. The natural frequencies accounting for spike swing are revealed to be in the ranges of (0.07 GHz, 0.12 GHz) or (0.26 GHz, 0.44 GHz) considering the effects of potential temperature elevation. Ultrasonic excitation is justified theoretically to be able to break the viral spikes in less than 180 ns in the way of frequency scanning through the range covering the natural frequency of the mode of spike swing.

Statement of significance

Using some physical methods to inactivate the new coronavirus in the environment is the key to preventing the spread of the virus. In this paper, it is found that the mutation of the new coronavirus would not change its spike vibration shape, accompanied with which the corresponding natural frequency fall into some certain range. Based on this, the frequency scanning strategy for the rapid ultrasonic inactivation of coronavirus is proposed and verified. This will help people end the new coronavirus pandemic as soon as possible, and can also be utilized analogously to the inactivation of similar pathogens.

CRediT authorship contribution statement

Cong Liu: Methodology, Investigation, Visualization, Writing – original draft. **Chen-Wu Wu:** Conceptualization, Methodology, Investigation, Supervision, Writing – original draft, Writing – review & editing.

Declaration of Competing Interest

The authors declare that they have no known competing financial interests or personal relationships that could have appeared to influence the work reported in this paper.

References

- [1] N. Davies, et al., *Science* 372 (2021) eabg3055, <https://doi.org/10.1126/science.abg3055>.
- [2] H. Tegally, et al., *Nature* 592 (2021) 438–443, <https://doi.org/10.1038/s41586-021-03402-9>.
- [3] T. Alpert, et al., *Cell* 18 (4) (2021) 2595–2604.e13, <https://doi.org/10.1016/j.cell.2021.03.061>.
- [4] Y. Hou, et al., *Science* 370 (2020) 1464–1468, <https://doi.org/10.1126/science.abe8499>.
- [5] G. Chand, et al., *Gene Rep.* 21 (2020) 100891, <https://doi.org/10.1016/j.genrep.2020.100891>.
- [6] Y. Cai, et al., *Science* 373 (2021) 642–648, <https://doi.org/10.1126/science.abi9745>.
- [7] J. Mateus, et al., *Science* (2021), <https://doi.org/10.1126/science.abj9853>.
- [8] T. Villa, et al., *Arch. Microbiol.* 203 (2021) 443–464, <https://doi.org/10.1007/s00203-020-02040-5>.
- [9] C. Wang, et al., *Arch. Microbiol.* 203 (2021) 443–464, <https://doi.org/10.1126/science.abd9149>.
- [10] P. Lelie, et al., *J. Med. Virol.* 23 (1987) 297–301, <https://doi.org/10.1002/jmv.1890230313>.
- [11] K. Tsen, et al., *J. Biomed. Opt.* 12 (6) (2007) 064030, <https://doi.org/10.1117/1.2821713>.
- [12] R. Cerf, et al., *Proc. Natl. Acad. Sci.* 76 (4) (1979) 1780–1782, <https://doi.org/10.1073/pnas.76.4.1780>.
- [13] S. Yang, et al., *Sci. Rep.* 5 (2016) 18030, <https://doi.org/10.1038/srep18030>.
- [14] B. Chen, et al., *Environ. Pollut.* 283 (2021) 117074, <https://doi.org/10.1016/j.envpol.2021.117074>.
- [15] J. Abraham, et al., *Rev. Med. Virol.* 30 (2020), <https://doi.org/10.1002/rmv.2115>.
- [16] G. Scherba, et al., *Appl. Environ. Microbiol.* 57 (7) (1991) 2079–2084, <https://doi.org/10.1128/aem.57.7.2079-2084.1991>.
- [17] M. Yao, H. Wang, *Nonlin. Dyn.* 106 (2021) 1425–1432, <https://doi.org/10.1007/s11071-020-06019-1>.
- [18] T. Wierzbicki, et al., *J. Mech. Phys. Solids* 150 (2021) 104369, <https://doi.org/10.1016/j.jmps.2021.104369>.
- [19] J. Kennedy, *Nat. Rev. Cancer* 5 (2005) 321–327, <https://doi.org/10.1038/nrc1591>.
- [20] S. Li, et al., *Biophys. J.* 100 (2011) 637–645, <https://doi.org/10.1016/j.bpj.2010.12.3701>.
- [21] M. Mateu, *Virus Res.* 168 (1–2) (2012) 1–22, <https://doi.org/10.1016/j.virusres.2012.06.008>.
- [22] I. Schaap, et al., *J. Biol. Chem.* 287 (49) (2012) 41078–41088, <https://doi.org/10.1074/jbc.M112.412726>.
- [23] T. Mukhopadhyay, et al., *Adv. Theory Simul.* 4 (2021) 2000291, <https://doi.org/10.1002/adts.202000291>.
- [24] H. Yao, et al., *Cell* 183 (2020) 730–738, <https://doi.org/10.1016/j.cell.2020.09.018>.
- [25] L. Casalino, et al., *ACS Central Sci.* 6 (2020) 1722–1734, <https://doi.org/10.1021/acscentsci.0c01056>.
- [26] J. Zhang, et al., *Science* 372 (2021) 525–530, <https://doi.org/10.1126/science.abf2303>.
- [27] T. Yang, et al., *Nat. Struct. Mol. Biol.* 28 (2021) 731–739, <https://doi.org/10.1038/s41594-021-00652-z>.
- [28] M. Kraemer, et al., *Science* 373 (2021) 889–895, <https://doi.org/10.1126/science.abj0113>.
- [29] J. Shang, et al., *Nature* 581 (2021) 221–226, <https://doi.org/10.1038/s41586-020-2179-y>.
- [30] H. Ewalds, R. Wanhill, *Fracture Mechanics*, Edward Arnold Ltd, London, 1984.
- [31] F. Fahy, P. Gardonio, *Sound and Structural Vibration*, Academic Press, Oxford, 2007.
- [32] O. Zienkiewicz, R. Taylor, *The Finite Element Method*, Butterworth-Heinemann, Oxford, 2000.